Structure determination of monolayer-by-monolayer grown $La_{1-x}Sr_xMnO_3$ thin films and the onset of magnetoresistance

R. Herger, P. R. Willmott,* C. M. Schlepütz, M. Björck, S. A. Pauli, D. Martoccia, and B. D. Patterson
Swiss Light Source, Paul Scherrer Institut, CH-5232 Villigen, Switzerland

D. Kumah and R. Clarke
Randall Laboratory of Physics and FOCUS Center, University of Michigan, Ann Arbor, Michigan 48109-1120, USA

Y. Yacoby
Racah Institute of Physics, Hebrew University, Jerusalem 91904, Israel

M. Döbeli
Ion Beam Physics, Paul Scherrer Institut and ETH-Zurich, CH-8093 Zurich, Switzerland
(Received 28 September 2007; published 1 February 2008)

Surface x-ray diffraction was used to determine the atomic structures of $La_{1-x}Sr_xMnO_3$ thin films, grown monolayer by monolayer on $SrTiO_3$ by pulsed laser deposition. Structures for one-, two-, three-, four-, six-, and nine-monolayer-thick films were solved using the Coherent Bragg rod analysis phase-retrieval method and subsequent structural refinement. Four important results were found. First, the out-of-plane lattice constant is elongated across the substrate-film interface. Second, the transition from substrate to film is not abrupt, but proceeds gradually over approximately three unit cells. Third, Sr segregates towards the topmost monolayer of the film: we determined a Sr-segregation enthalpy of −15 kJ/mol from the occupation parameters. Finally, the electronic bandwidth W was used to explain the onset of magnetoresistance for films of nine or more monolayers thickness. Resistivity measurements of the nine monolayer-thick film confirm magnetoresistance and the presence of a dead layer with mostly insulating properties.

DOI: 10.1103/PhysRevB.77.085401 PACS number(s): 68.47.Gh, 61.05.cp, 81.15.Fg, 75.47.Gk

I. INTRODUCTION

Ferromagnetic manganites were first investigated by Jonker and van Santen in 1950, but have attracted renewed interest in recent years since the discovery that they exhibit colossal magnetoresistance (CMR).[1,2] Doped manganites with the perovskite structure and chemical composition $RE_{1-x}AE_xMnO_3$, where RE is a rare earth and AE is a divalent alkaline earth, show rich phase diagrams, due to the complex interplay of charge, spin, lattice, and orbital degrees of freedom.[3,4] Their interesting physical properties have not only triggered renewed scientific interest in these compounds, but also show potential for many technological applications such as spin electronics or magnetic sensors. Thin films are best suited for these demands.

The ongoing trend of miniaturization means that novel materials in the form of thin films are very important for any technological application. Surface and interface effects can set a lower limit to downsizing devices that exploit bulk effects. These mainly structural considerations become particularly important in ultrathin films, where surface and interface relaxations can involve a significant fraction of the film volume and hence fundamentally change the physical properties. An exact knowledge of the atomic positions is therefore of great importance for the design of nanoscaled devices.

Bulk $La_{1-x}Sr_xMnO_3$ (LSMO) at an optimal doping of $x=1/3$ shows the transition from a paramagnetic insulator to a ferromagnetic metal at temperatures as high as $T_C=370$ K.[4] The Mn site has a mixed valence state of x Mn^{4+} (holes) and $(1-x)$ Mn^{3+}, leading to degenerate high-spin t_{2g}^3 and $t_{2g}^3e_g^1$ states of the MnO_6 octahedra, respectively, due to the large Hund exchange energy of $J_H \approx 2.5$ eV in the crystal field. The electrons can hop between adjacent Mn ions, as described by Zener's double-exchange mechanism[5] and thus mediate the long-range ferromagnetic ground state of the metallic conductor. Additionally, as the electronic ground state of the Mn^{3+} sites is degenerate, a Jahn-Teller distortion breaks the octahedral symmetry and lowers the energy.[6]

In thin films, however, the transport properties of LSMO change dramatically. The typical shape of the metal-insulator transition of the bulk changes to a more semiconductorlike behavior of the resistivity curve in ultrathin films, with resistivities in the low temperature regime being approximately four orders of magnitude higher. This has been explained by the presence of an electrical "dead layer" at the substrate-film interface.[7–9] Nevertheless, such films still exhibit magnetoresistive behavior.[7] Our intention is thus to use exact atomic coordinates to correlate the structure with the transport properties, in order to determine a minimum thickness for the onset of magnetoresistance.

In this work, we present a detailed structure determination via surface x-ray diffraction (SXRD) of thin LSMO films of 1-, 2-, 3-, 4-, 6-, and 9-monolayer (ML) thickness, grown by pulsed laser deposition (PLD) pseudomorphically on (001) $SrTiO_3$ (STO, cubic lattice constant $a_{STO}=3.905$ Å). A structural study of different film thicknesses has enabled us to monitor the evolution of the growth of thin films with sub-Å resolution, revealing interesting structural features.

The main results of the structure determination are (i) the observation of a dilation of the interface perpendicular to the

surface, in contrast to the compression that one would intuitively expect due to the tensile in-plane stress of LSMO [quasicubic lattice constant of $a_{LSMO}=3.875$ Å ($x=0.35$) (Ref. 4)] grown on STO; (ii) the formation of a nonabrupt interface that is used to derive a general picture of how the film stoichiometry becomes established; (iii) the enrichment of Sr in the topmost layer of the film surface with an approximate estimate of the segregation enthalpy based on occupation parameters; and (iv) the fact that magnetoresistance can be observed in films with nine or more ML thickness, explained by considerations of the electronic bandwidth using the structural data and by comparison with the bulk properties.

II. METHODS

A. Experiment

1. Pulsed laser deposition

LSMO thin films were grown in an *in situ* PLD chamber mounted on a surface x-ray diffractometer.[10] The films were deposited on STO(001) substrates with low vicinality ($<0.1°$) prepared by an established chemical and thermal treatment to ensure TiO_2 termination.[11,12]

We used the fourth harmonic of a Nd:YAG laser (10 Hz, 266 nm, 5 ns, 2 J cm^{-2}) as the ablation source, in conjunction with a synchronized N_2O gas pulse (1.5×10^{-2} Pa, average pressure) and an O_2 background (2×10^{-2} Pa). These conditions led to films of high crystallinity.[13]

Film growth was monitored by recording the reflected x-ray signal at the (0 0 1/2) position of the specular crystal truncation rod (CTR).[14] The laser was operated in an interrupted mode, in which short bursts of ablation (typically 12 shots, the minimum required to ensure the conservation of the chosen stoichiometry of $x=0.35$) are separated by a period of several tens of seconds, in order to let the surface thermally relax. After deposition, the films were quenched in oxygen.

Here, we report on films that are 1, 2, 3, 4, 6, and 9 MLs thick. Henceforth, we refer to a film of y ML thickness (i.e., the substrate surface covered by an LSMO layer of exactly y unit cells in height) as LSMO y, e.g., the 4-ML-thick film is LSMO 4. The films were grown on three different STO substrates 1, 2, and 3, as described in Table I.

2. Surface x-ray diffraction

Surface x-ray diffraction experiments were carried out at the surface diffraction station of the Materials Science Beamline at the Swiss Light Source, Paul Scherrer Institut.[15] The growth chamber contains a large beryllium window,[10] enabling *in situ* data acquisition. The (2+3) surface diffractometer is equipped with a fast, single photon-counting 2D x-ray pixel detector. We used 1-Å synchrotron radiation and a fixed incidence angle of 0.15°, slightly below the critical angle of 0.20°, in order to enhance the surface signal.

After every deposition, we recorded a large SXRD data set, typically consisting of ten inequivalent and about five equivalent CTRs (see Table I for details). From the pixel images, the integrated intensities were extracted and standard geometrical correction factors applied.[16] Thus we obtained about 400 nonequivalent structure factors for each thickness, resulting in systematic errors ranging from 5 to 17 %, primarily attributable to mechanical distortions (e.g., bending of the substrate) produced by the heater/clamping mechanism.

TABLE I. Details of SXRD data sets and refinement parameters. Film thicknesses are given in MLs and STO denotes the used substrate. The number of inequivalent (ineq.) and equivalent (eq.) structure factors (SFs) are given with the number of measured CTRs in brackets. ϵ is the systematic error and P is the number of fit parameters used with the resulting oversampling factor (O). The final R factor $R(|F|)$ after structure refinement is given. The surface occupation (SO) is in fractions of a ML.

		SFs (CTRs)						
Film	STO	Ineq.	Eq.	ε (%)	P	O	$R(\|F\|)$ (%)	SO
1	1	369(10)	211(5)	17.1	36	10.3	13.3	0.897
2	1	408(11)	316(9)	9.6	48	8.5	8.2	0.920
3	1	369(10)	157(4)	5.3	60	6.2	8.3	0.891
4	2	418(11)	303(9)	16.4	72	5.8	16.4	0.925
6	3	375(10)	315(6)	11.2	96	3.9	10.3	0.999
9	3	1029(10)	0(0)	11.2[a]	132	7.8	10.2	1.005

[a]Due to the lack of equivalent reflections, ε was assumed to be the same as for LSMO 6 on the same STO sample 3.

The data span reciprocal space in $|h|$ and $|k|$ from 0 to 4. Perpendicular to the surface, we selected reflections with $0.5\leq l<3$, in order to account for the sampling resolution along l, the quality of the STO substrates, and the angle of incidence, as reasoned elsewhere.[17] None of the films showed reconstructions.

3. Ex situ characterization

(*a*) *Rutherford backscattering*. Rutherford backscattering (RBS) experiments were carried out using a 2-MeV ^{4}He beam and a silicon surface barrier detector at a scattering angle of 165°.[18] The background was subtracted using a recently developed fitting procedure.[19] For thicker films of the order several tens of nm (not presented here) grown using the same conditions as described in Sec. II A 1, the elemental composition could be determined using the RUMP program.[20] For very thin films consisting of only a few MLs, however, the RBS analysis for Sr and O fails. Nevertheless, the stoichiometry could be obtained by element-specific integration of the backscattering signal of La and Mn and their correlation to the integrated signals of the thicker films, under the assumption that the backscattering yield for thin films is proportional to that for thick, more bulklike films.

In addition, RBS channeling experiments yielded information on the growth quality and crystallographic defects such as dislocations or interface roughness. A representative channeling spectrum of a 130-nm-thick LSMO film can be found in Ref. 13.

(*b*) *X-ray reflectivity*. We recorded x-ray reflectivity (XRR) curves at a wavelength of 1 Å in order to determine the thickness of LSMO 6 and LSMO 9. The reflected signal for each incident angle was integrated and corrected for the

footprint of the x-ray beam on the sample surface. The reflectivity curves were fit using the program GENX.[21]

(*c*) *X-ray diffraction*. Laboratory-based $\theta-2\theta$ scans using Cu $K\alpha$ radiation confirmed single crystal growth along the (001) axis.

(*d*) *Resistivity*. The resistivity was measured using the four-point method in a customized sample holder. We used a Quantum Design model 6000 physical properties measurement system (PPMS) to measure the electrical resistance R without and with an applied field of $B=5$ T perpendicular to the film surface. Every point was measured 25 times, and the standard deviation was calculated. Before the resistivity measurements, LSMO 3, 4, and 9 were annealed in pure, flowing oxygen at 900 °C for 3 h in order to enhance the transport properties of the thin film.

B. Structural analysis

Coherent Bragg rod analysis (COBRA) is a direct phase-retrieval algorithm for SXRD data.[22] The COBRA method is generally applicable to systems that are periodic in two dimensions, aperiodic in the third, and commensurate with the underlying substrate. COBRA provides a 3D electron density map of the system with sub-Å resolution. For each film thickness, a reference structure consisting of an undistorted film and substrate with bulk positions and nominal thickness and composition was used. Convergence was achieved after three to four small COBRA phasing iterations.[22,23] In Fig. 1, the COBRA result for LSMO 4 is presented as an example.

To obtain more precise occupancy results, the atomic positions and the occupancies of the film layers determined by COBRA were used as a starting model for subsequent structure refinement in the FIT program.[24] Structural refinement robustly converged for a given film thickness. All thicknesses were modeled using consistent conditions (i.e., concerning symmetry, fit parameters, etc.) and thus the refined models enable one to directly compare the results. Optimization was carried out by minimizing the crystallographic R factor.[25] It is emphasized that without the initial COBRA phasing, there are too many unknown parameters for the fitting and refinement approach alone to converge on a viable solution.

The structures were modeled as follows. Atoms were allowed to move only in the z direction, i.e., perpendicular to the surface, according to the *p*4*mm* surface symmetry. The positive z direction (in units of bulk STO unit cells) was defined as pointing out of the surface. The positions of all the film atoms and the three top MLs of bulk STO ($z>-3$, with the top substrate TiO_2 layer as the nominal zero position) were refined. It was found that fitting the positions of La independently from that of Sr on the same site, and Ti independently of Mn, made no significant improvements to the fit. Hence La and Sr, as well as Ti and Mn, each used a common position parameter. Every atom from $z>-1$ up to the surface was assigned an individual isotropic Debye-Waller (DW) factor. For $z\leq-1$, the sites of each atom type had element-specific isotropic DW factors for Sr, Ti, and O. The occupation parameters of La and Sr, and Ti and Mn were refined with the restriction that the total occupation per site had to be unity. We modeled an incomplete (or "overcomplete") ML coverage that might occur in the PLD growth process by allowing the top *monolayer*[26] of the film to have a noninteger occupation [see the surface occupation (SO) column in Table I]. This parameter also accounts for possible surface roughness, although the root mean square roughness is known to be only 1 to 2 Å for films of several tens of nanometers thickness.[7,27]

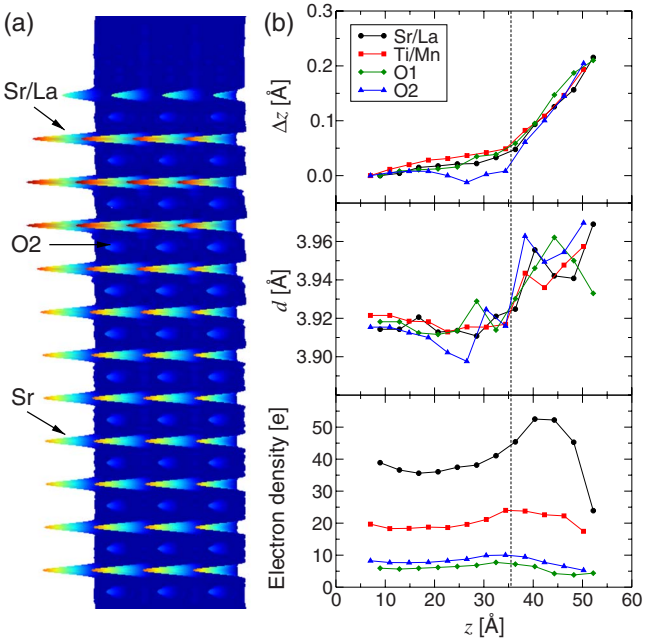

FIG. 1. (Color online) COBRA results for LSMO 4. (a) The electron density (ED) map obtained by the COBRA phasing method, showing the plane along z containing the La, Sr, and O2 atoms. (b) The cumulative displacement Δz of the atoms from the reference frame of bulk STO (top), the distances d between neighboring atoms of the same element across the substrate-film interface (middle), and the integrated electron densities of the Gaussian-like features in the ED maps (bottom). Uncertainties in Δz and d are estimated to be ± 0.03 Å, while the electron densities are accurate to $\pm 5\%$.

III. RESULTS AND DISCUSSION

A. Film characterization

1. Thickness of the films

For all LSMO films, the thickness was apparent from the growth oscillations. For the thicker films, however, we additionally used XRR to verify the thickness. Fitting with GenX gave 5.6(2) and 9.1(2) MLs for LSMO 6 and LSMO 9, respectively, using the bulk LSMO lattice constant. The XRR fits also reveal that the films consist of an approximately 22-Å-thick interface region of higher optical density and, for LSMO 9, a second, graded, less dense surface layer (up to 20% less at the surface)[28] of approximately 10 Å depth, which is probably caused by surface roughness and/or incomplete monolayer coverage. The XRR result for LSMO 6 is not in perfect agreement with the nominal 6 MLs. From

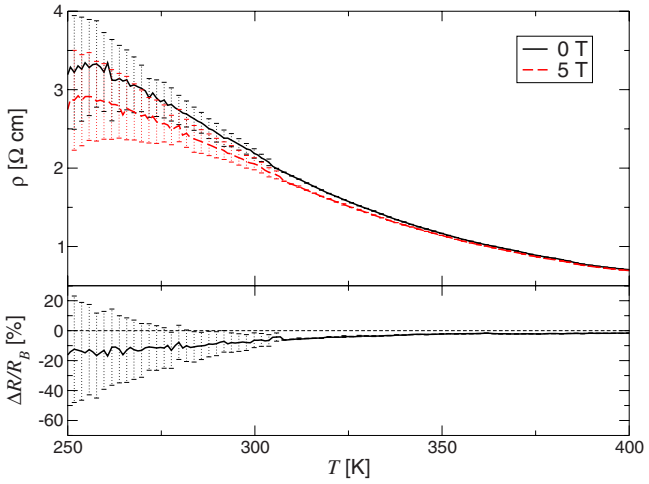

FIG. 2. (Color online) Top: Resistivity curves of LSMO 9 without magnetic field (solid black) and at $B=5$ T (dashed red). Bottom: Magnetoresistance ratio $\Delta R/R_B=(R_B-R_0)/R_B$. The dashed line is a guide to the eye and indicates zero magnetoresistance. Only every second error bar is drawn to improve the readability.

Table I and the growth oscillations, we have to conclude that this film has a thickness very close to 6 MLs. This is also supported by the fact that LSMO 9 is the continuation of the growth of LSMO 6.

2. Resistivity measurements

Experimental resistivity curves of LSMO 9 are shown in Fig. 2.[29] The resistivity ρ is relatively high, as would be expected for a film of only 9 ML thickness, and shows semiconducting behavior. Applying a field of $B=5$ T reduces ρ, i.e., we see a magnetoresistive effect. Note that the error bars (i.e., the standard deviations) below 310 K suddenly increase. We attribute this to the voltage limit of the PPMS. We get a negative magnetoresistance ratio $\Delta R/R_B=(R_B-R_0)/R_B=-7\%$ at 310 K. This value is far from being "colossal," but consistent with other experimental observations for comparably thin films.[7,8]

The curves do not show the usual metal-insulator transition that one might expect for thicker, bulklike films. Instead, they resemble more semiconducting behavior, indicating the presence of an electrical dead layer at the substrate-film interface. Recent theoretical investigations reveal this to be an intrinsic phenomenon at a metal-insulator interface.[30] These dead layers were found all to have similar thicknesses, independent of the substrate used: 5 (12), 5 (12), 3 (8), and 4 (10) nm (MLs) for LSMO grown on STO, $LaAlO_3$, $NdGaO_3$, and MgO, respectively.[7–9] Interestingly, Sun *et al.*[8] ruled out that the presence of these dead layers is caused by strain and concluded that the substrate-film interface and/or the surface must be chemically or structurally altered in LSMO thin films. Liao *et al.*[7] gave a possible explanation for the simultaneous presence of magnetoresistance and high resistivity. From the observation of a spatially inhomogeneous metal-insulator transition, they concluded that phase separation leads to ferromagnetic metallic domains embedded in an insulating framework of the dead layer.

B. Structure

We present three selected CTRs [$(11l)$, $(22l)$, and $(32l)$] for each thickness plus the fit intensities in Fig. 3. The R factors range from 8.2 to 16.3 % (see Table I). The atomic coordinates and occupation parameters of the films are available online.[31] The discussion in the following sections is based on these data and will lead to the four main results of this work.

The surfaces of our thin films appear to have a low defect density, judged from inspection of the DW factors. Moreover, high-quality growth on STO can be achieved even for

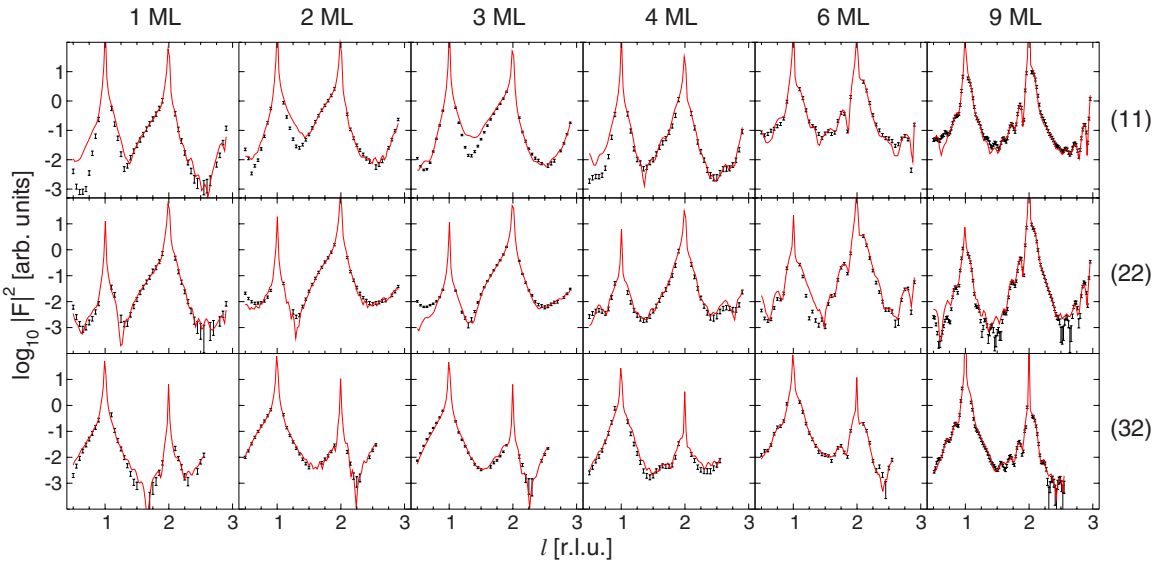

FIG. 3. (Color online) Sets of SXRD data (black) and calculated intensities (red) for different film thicknesses as labeled. For representation, three rods of the data files were selected: $(11l)$ top, $(22l)$ middle, and $(32l)$ bottom.

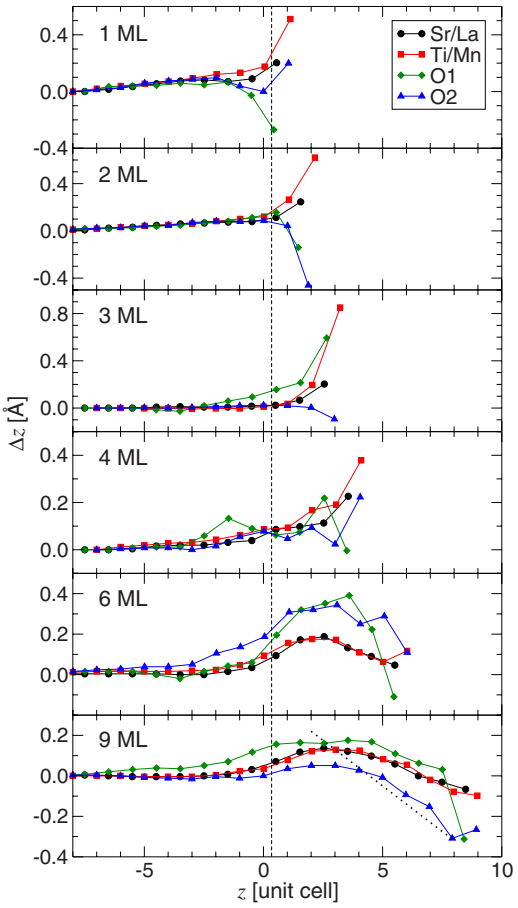

FIG. 4. (Color online) The cumulative displacements Δz of the atoms from the reference frame of the positions for bulk STO. The zero position in z represents the top TiO_2 layer of bulk STO with the nominal interface indicated by the dashed line. Color and symbol code: Sr/La=black •, Ti/Mn=red ■, O1=green ♦, O2=blue ▲. All film thicknesses show an elongation of the out-of-plane lattice constant at the interface. Results for metallic sites are estimated to be accurate to ±0.03 Å, with the caveat that the positions in the topmost ML of the thinnest films (1–3 MLs) are likely to have significantly larger uncertainties, as are the oxygen displacements. Thinner films exhibit a more pronounced increase in the lattice constant than thicker films. The dotted line for LSMO 9 has a slope of $\Delta z=-0.09z+0.4$ and indicates the LSMO lattice constant for strained bulk above $z\geq 3$ MLs, as detailed in the text.

thick LSMO films (i.e., several tens of nanometers), as can be seen from our RBS channeling results and the clear Kickuchi lines in the reflection high-energy electron-diffraction pattern[13] or by atomic force microscopy.[7,27]

C. Substrate-film interface

One of the main results of this work is the unusual behavior of the substrate-film interface. Tensile stress in-plane of the smaller LSMO unit cell grown on STO would, on its own, lead to a *decrease* in the out-of-plane lattice constant c. We see, however, the opposite phenomenon (Fig. 4): All our films show an *increase* in the out-of-plane lattice constant across the interface, with a maximum deviation from bulk STO after about 3 MLs. For films thicker than 3 MLs, this dilatory layer is capped by a layer where c decreases again. If we were to assume a *strained* bulk lattice constant for films thicker than 3 MLs ($z\geq 3$), the slope would be given by −0.09 Å. This is represented by the dotted line in Fig. 4. We note that $c>c_{\mathrm{LSMO,strained}}$, i.e., the film is less strained than expected from this simple model taking only in-plane compressive strain into account.

Figure 4 also gives information on the reliability of the atomic positions, as the six films were grown on three different substrates. For the metallic sites, the positions are reproduced to within ±0.03 Å. The results for oxygen, with its low x-ray scattering power are likely to be significantly less reliable. Note also that the cumulative displacement in the very uppermost monolayer (i.e., at the growth surface) of the thinnest films (1–3 MLs) may be less reliable because of surface roughness and/or incomplete occupancy.

An important issue to be addressed is interfacial roughness. The refined DW factors at the interface are comparable to the tabulated bulk values,[32] indicating low uncertainties in the atomic positions. Sometimes, we note increased DW factors for Sr in the film. A possible explanation for this could be the preference of Sr to segregate, as discussed in Sec. III E. Our RBS channeling results for thicker films (≈130 nm) reveal almost no interfacial crystallographic defects.[13] We can therefore conclude that the interface roughness is low and plays a negligible role for any explanation of the behavior of the film-substrate interface.

As mentioned above, elongation of c at the interface cannot be explained by strain alone. A more likely explanation could involve the presence of ions in lower oxidation states. Such atoms have larger ionic radii and could account for the observed dilation. We will address this in the next section in more detail.

Finally, fitting of the (002) Bragg peak of STO from laboratory-based $\theta-2\theta$ scans using Voigt line profiles corroborated the increase in the out-of-plane lattice constant in LSMO 3, 4, and 9. Only LSMO 9 additionally showed a significant signal attributable to a c smaller than c_{STO}, which probably can be associated with the upper MLs of the film.

D. Stoichiometry

We present the change in occupancies for the metallic sites across the substrate-film interface in Fig. 5. The transition from substrate to film is not abrupt, but proceeds gradually over two to three MLs and already starts in the nominally top ML of the STO substrate.

The COBRA results give clear evidence for the gradually changing interface (Fig. 1). It is unlikely that this effect is merely an artefact of the COBRA analysis, based on the following arguments. Ultra thin two-dimensional (2D)-grown films of the order of several MLs tend to mimic the substrate surface, i.e., flat substrate surfaces will translate to flat film surfaces. The COBRA results reveal such a behavior: The integrated electron density (ED) drops off very sharply within half a ML at the film surface, suggesting a flat film surface and a (initially) flat substrate surface. However, the ED gradually increases over approximately 3 MLs, sug-

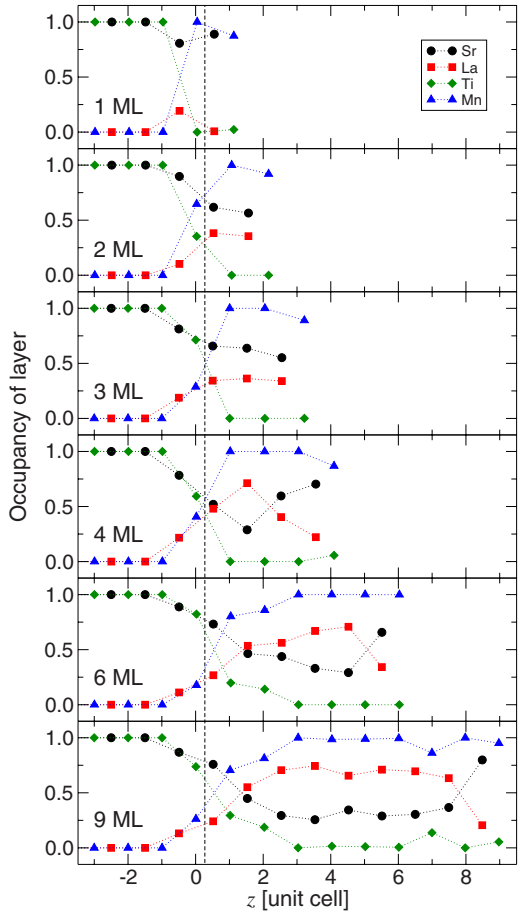

FIG. 5. (Color online) Occupancies across the substrate-film interface (dashed line) for different film thicknesses. The change in stoichiometry takes place over approximately three unit cells. Sr =black •, La=red ■, Ti=green ♦, Mn=blue ▲.

gesting that the gradual change of the stoichiometry across the interface is real.

We first focus on the Sr/La evolution. We use x' to denote the Sr content of a specific ML (and La=$1-x'$). For the three thicker films, we see x' changing from 0.85 to 0.4 as z increases from −0.5 to 1.5.[33] Above $z=1.5$, $x' \approx 0.3$, up to the topmost layer, where x' suddenly increases again and reaches a typical value of $x'=0.72$. This can be explained by preferential Sr segregation and will be discussed below. For the three thinnest films, the crossover to more La than Sr does not take place. A possible explanation could be that Sr segregation competes with the establishment of the "nominal" stoichiometry ($x'=0.35$). The disagreement for LSMO 3 between the stoichiometry determined by structural refinement and by RBS (Table II) is probably because with only 3 MLs, we are close to the limit of depth resolution of RBS.

We turn now to the transition of Ti to Mn. The two elements are very hard to distinguish with nonresonant x-ray techniques, as their atomic numbers only differ by 3. The fact that their occupation parameters have distinct values and show consistent trends can be explained with the accurate approximation of the atomic form factors in FIT and the reliability of our SXRD data. There are, however, limitations,

TABLE II. Average occupation parameters determined with FIT compared with RBS results for La and Sr.

	FIT		RBS	
LSMO	La	Sr	La	Sr
3	0.43	0.57	0.69	0.31
4	0.52	0.48	0.64	0.36
9	0.59	0.41	0.62	0.38

as can be seen in Fig. 5. The transition from Ti to Mn seems to indicate an enrichment of Mn, whereby the number of MnO_2 layers exceeds the nominal film thickness in MLs by 1, as can be seen by the Mn-rich ML of LSMO 1 below the nominal interface. However, it remains unclear where this extra Mn should come from. A more likely explanation for this could be the presence of additional Ti in the interface region, in combination with the fact of similar scattering behavior of Mn and Ti when probed with x rays. In Ref. 12 we found the STO substrate under thin film growth conditions to be terminated with a double TiO_2 layer. Moreover, growth oscillations show a peculiar behavior immediately after starting deposition, which could be interpreted as a fingerprint of the incorporation of the TiO_2-double layer into the film structure (see, for example, Fig. 1 in Ref. 14). From the COBRA results, we do not see that a TiO_2-double layer, as proposed in Ref. 12, is present at the substrate-film interface. But the integration of the additional TiO_2-layer material into the film structure remains an interesting suggestion. More work on the growth modes of LSMO thin films has to be carried out to resolve this issue unambiguously.

We are now able to summarize the evolution of the stoichiometry for LSMO thin films. Figure 6 shows a general depth profile with typical values for metal occupations across the interface, in the film, and at the surface for an idealized 9-ML-thick LSMO film, based on the average experimental values in Fig. 5.

As we recently showed in the case of $LaAlO_3$ on TiO_2-terminated STO,[34] the valence state of the metal ion in

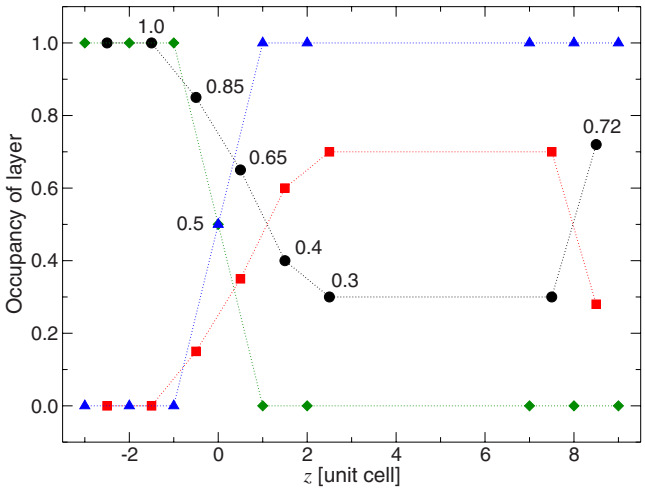

FIG. 6. (Color online) Evolution of the stoichiometries for an idealized film of 9-ML thickness. Sr=black •, La=red ■, Ti=green ♦, Mn=blue ▲. The dotted lines are guides to the eye.

the center of the oxygen octahedron is crucial to explain the dilation across the film-STO interface. Above 2.5 MLs (where we also observe the dilation maximum), we note that according to the general picture in Fig. 6, the La^{3+} occupation is established. We thus also have the highest concentration of (high-spin) Mn^{3+} that has an ionic radius 0.115 Å larger than Mn^{4+}.[35] Moreover, the films seem to be Mn rich at the interface, which would explain the increase of c at the interface and the subsequent decrease after the interfacial region. But the argument would still hold if instead of Mn a higher concentration of Ti was assumed, due to the additional Ti from the double layer, as the ionic radius of Ti^{3+} is 0.065 Å larger than that of Ti^{4+}. Either way, an enrichment of trivalent metal (Me^{3+}) species at the interface would help to explain the elongation of the out-of-plane lattice constant in the interface region.

Electrostatic considerations help to further corroborate any enrichment of the trivalent sites across the interface. The exchange of Sr and La cations lead to the formation of a dipole moment with the electric field and electric potential both being nonzero in the film. The trivalent species can minimize the electrostatic energy, if we require the electric field to be minimized and the electric potential to be zero at the film boundaries. We carried out such a minimization for the four interfacial MLs of LSMO 9 ($0 \leq z \leq 3$) and found that the enrichment of the trivalent species above the nominal interface is highest around $z=1$, leading to full occupation with Me^{3+}, with decreasing occupancy above and below. Note that the position of this maximum coincides with the highest gradient of the metal sites of LSMO 9 in Fig. 4. The minimization of the electrostatic energy thus supports the picture of a Me^{3+}-rich interface. However, a quantitative discussion of the evolution of the Ti^{3+}/Mn^{4+} ratio across the interface is beyond the accuracy of the used ionic radii,[35] in order to explain the experimentally observed lattice constants.

E. Strontium segregation

The film surface consistently shows a higher Sr content in the topmost ML than the film average. We attribute this to Sr segregation. The effect of segregation of the divalent site has been discussed before and was suggested to either behave exponentially[36] or occur exclusively in the outermost layer.[37,38] We cannot infer an exponential behavior from the data shown in Fig. 5, but do support a Sr-rich topmost unit cell. Moreover, the nature of the terminating layer at the film surface, either SrO (Ref. 37) or MnO_2 (Ref. 39), has been discussed in the literature. The COBRA results, on which the fits are based, demonstrate that the surface is terminated with a MnO_2 atomic layer. There is only a negligible amount of extra material above the nominal surface ML, in agreement with what one would expect for PLD growth on TiO_2-terminated STO substrates. Our FIT results support this: the addition of a partially occupied extra Sr/La-O atomic layer on top of the surface led to coverages at most of the order of the uncertainty of a laser burst, i.e., 7 to 8 % of a ML. Note also that the addition of such a sparsely occupied overlayer in the fit had no effect on the Sr enrichment of the complete (real) surface beneath it. In other words, the Sr enrichment is real and cannot be an artefact caused by a partially occupied overlayer.

Indeed, we can explain the observed Sr segregation by an intrinsic growth phenomenon, since LSMO 9 is a continuation from LSMO 6, i.e., both are grown on the same STO sample, and both films show a Sr enrichment only at the surface layer of the film. A surface segregation phenomenon suggests different enthalpies of the surface and film. We can write the total free energy F for a multicomponent system using a simple statistical model of segregation:[40]

$$F = \sum_i n_i^s g_i^s + n_i^f g_i^f - k_B T \ln \Omega, \tag{1}$$

where n_i^s and n_i^f are the number of surface and film atoms of type i, and g_i^s and g_i^f are the individual Gibbs free energies, respectively. k_B is the Boltzmann constant, T is the temperature, and Ω is the entropy due to the mixing of the compounds. The competition of minimizing the free energy terms of the individual components and maximizing the entropy causes the segregation.

We can derive an Arrhenius expression for the two component system, depending on the occupation x:

$$x_s = x_f \exp\left(\frac{-H}{k_B T}\right), \tag{2}$$

where $x_s = n_{\mathrm{Sr}}^s / n_{\mathrm{La}}^s$ and $x_f = n_{\mathrm{Sr}}^f / n_{\mathrm{La}}^f$ depend on the surface and film stoichiometry, respectively, and H is the segregation enthalpy. Using the values we summarized for the stoichiometry evolution in Fig. 6 ($x_s=2.57$, $x_f=0.429$), we obtain $H=-15$ kJ/mol (or -0.16 eV for a Sr site) for the segregation of Sr towards the film surface. Moreover, any kinetic barrier can be easily overcome by the energy transfer from the impinging particles of typically 5–25 eV kinetic energy during PLD growth.[41]

F. Bandwidth

At a fixed hole density x, the properties of the manganites are affected by distortions of the ideal cubic geometry, qualitatively expressed by the tolerance factor $\Gamma = (r_A + r_O)/[\sqrt{2}(r_B + r_O)]$. The transport properties depend on the overlap of the Mn sites with the O $2p$ orbitals, which in turn is determined by the Mn-O-Mn angle ϕ. $\phi < 180°$ result in a reduced electron hopping amplitude, proportional to $\cos \phi$.[42] In the case of LSMO, the tolerance factor $\Gamma = 0.98$ (for $x = 0.35$), and $\phi < 180°$, and the tendency towards charge localization increases. Furthermore, in the Hubbard picture, the electron hopping term t is not only dependent on the bond angle ϕ, but also on the length of the Mn-O bond as $1/(d_{\mathrm{Mn\text{-}O}})^\alpha$, where $\alpha > 1$.[43] We therefore expect changes in T_C when ϕ and/or $d_{\mathrm{Mn\text{-}O}}$ change. This simple picture qualitatively explains the different Curie temperatures of $T_C = 370$ K, $T_C = 250$ K, and $T_C = 100$ K observed at a doping level of $x=0.3$ in $La_{1-x}Sr_xMnO_3$ ($\Gamma = 0.98$), $La_{1-x}Ca_xMnO_3$ ($\Gamma = 0.97$), and $Pr_{1-x}Ca_xMnO_3$ ($\Gamma = 0.92$), respectively.[35,44]

The electronic bandwidth W is directly proportional to the electronic hopping term t in the Hubbard model, i.e., the

ability of the Mn^{3+} e_g electrons to interact with the neighboring Mn^{4+} site via the O $2p$ orbital in order to develop the long-range ferromagnetic ordering in these materials. As a rule of thumb, the transition temperature T_C from a paramagnetic-insulating to a ferromagnetic conducting state increases with larger W. Note that this is usually accompanied by a reduction of the magnetoresistive effect.

The bandwidth W is influenced most by two relatively easily accessible structural quantities: the angle ϕ of a Mn-O-Mn bond and the Mn-O bond length $d_{\text{Mn-O}}$. For perovskite structures, W is a straightforward result of the tight-binding approximation. Empirically, the dependence of W on the bond angle and bond distance is given by[45]

$$W \propto \frac{\cos \omega}{(d_{\text{Mn-O}})^{3.5}}, \tag{3}$$

where $\omega=(\pi-\phi)/2$. Note that for calculations, average values for ϕ and $d_{\text{Mn-O}}$ are usually taken, as one is interested in W for the complete layer of material. In the bulk, $\phi=166°$,[44] whereas the films of this work had bond angles $162<\phi<176°$. Moreover, as we pointed out in Sec. III C, the oxygen positions are less accurately determined compared to the metallic sites. Thus a modification of Eq. (3) probably leads to more reliable results under the assumption that $\sin \phi/2 \approx 1$:

$$W \propto \frac{1}{(d_{\text{Mn-Mn}}/2)^{3.5}}, \tag{4}$$

where $d_{\text{Mn-Mn}}/2$ is taken as the estimate for $d_{\text{Mn-O}}$.

Using Eq. (4), the refined atomic positions were taken to calculate the electronic bandwidth W for different film thicknesses, both ML for ML [Fig. 7(a)], and $\bar{W}$, averaged and weighted for different Mn occupations [Fig. 7(b)]. For comparison, W was calculated using the bulk LSMO lattice constant.

For the three thinnest films in Fig. 7(a), W is either significantly below the bulk value (LSMO 1) or rapidly decreasing (LSMO 2 and 3). LSMO 3 indeed had a resistance too high to be measured using our four-point setup. LSMO 4 has bandwidths comparable to that of the bulk. However, we could not measure any electrical conductance across LSMO 4. Whether this is due to insufficient experimental sensitivity or because this film is in fact insulating cannot be assessed. For the two thickest films, W is very close to the bulk value. Additionally, the averaged bandwidth $\bar{W}$ in Fig. 7(b) shows that for the thinner films (LSMO 1–4), the bandwidth is quite different from the bulk value. On the other hand, $\bar{W}$ for the two thickest films is very close to the bulk value. This suggests that magnetoresistive behavior becomes established between 6 and 9 MLs. The onset of magnetoresistive behavior of films of a thickness of 9 or more MLs can therefore be expected, and was indeed experimentally found in this work.

It is important to note that the mostly insulating properties of the surface when measuring the electrical resistance do not exclude the existence of magnetoresistance, as can be seen in Fig. 2 and in other experimental observations.[7] We thus can confirm that the presence of an electrical dead layer does not imply an absence of magnetoresistance.

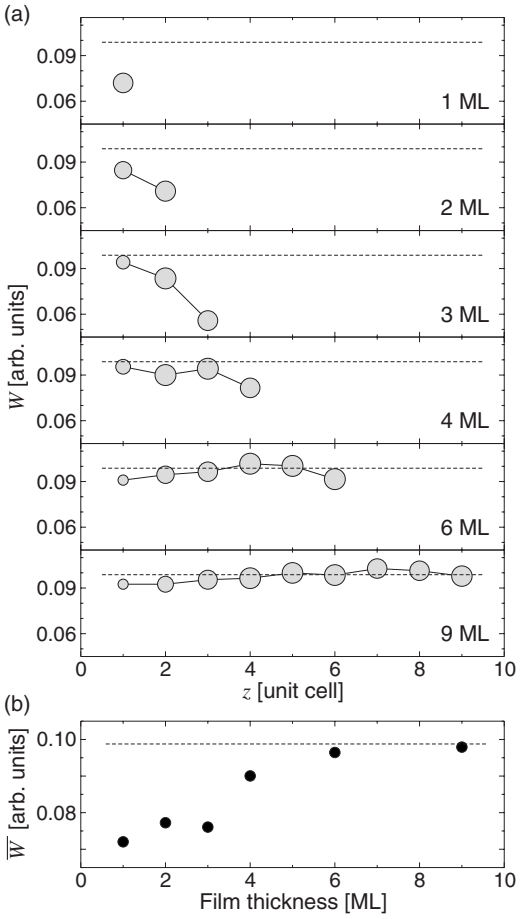

FIG. 7. Electronic bandwidth according to Eq. (4) for different film thicknesses based on the refined structure data: (a) W as a function of z calculated ML for ML with the size of the circles representing the weight of this particular data point; or (b) averaged and weighted for each film thickness. The dashed lines indicate bulk LSMO.

Finally, we note that the last data point of W in Fig. 7(a) is always somewhat lower compared to the next to last point. A possible explanation could involve the tendency of Sr to segregate towards the surface. This leads to a lower concentration of e_g electrons (and accordingly a higher hole concentration), which is reflected in the lower W value at the film surface. This might have important consequences for other experimental techniques probing mainly the surface such as x-ray photoelectron spectroscopy, and helps to explain angle-resolved photoemission data on this system.[46]

IV. CONCLUSIONS

We grew $La_{1-x}Sr_xMnO_3$ ($x=0.35$) thin films monolayer by monolayer on $SrTiO_3(001)$ with thicknesses of 1, 2, 3, 4, 6, and 9 MLs using pulsed laser deposition. We recorded large sets of structure factors for each film *in situ* by surface x-ray diffraction. The structures were analyzed using the di-

rect method technique COBRA and subsequent refinement of the atomic positions.

We observe an inherent dilation of the substrate-film interface perpendicular to the surface. The atomic positions of the substrate-film interface are well defined, indicative of low roughness. However, the transition from substrate to film is not abrupt: The stoichiometry changes over approximately three unit cells. The MnO_2-terminated film surfaces are Sr enriched in the topmost monolayer, due to a segregation process. This enthalpy is estimated to be of the order of -15 kJ/mol (or -0.16 eV/Sr). Using the refined atomic positions, we calculated the electronic bandwidths for comparison with bulk LSMO. This led to the suggestion of an onset of magnetoresistance of nine or more MLs. The resistivity measurements for the 9-ML-thick LSMO film indeed confirm magnetoresistance, but they also indicate the presence of an electrically insulating dead layer, in agreement with other experimental observations for such very thin films.

ACKNOWLEDGMENTS

We are indebted to E. Dagotto for his invaluable comments on the manuscript. Fruitful discussions with O. Bunk and J. Krempasky are gratefully acknowledged. We thank S. Weyeneth from the University of Zürich, Switzerland, for his assistance in the resistivity measurements and his help in interpretation of the results. Support of this work by the Schweizerischer Nationalfonds zur Förderung der wissenschaftlichen Forschung and the staff of the Swiss Light Source is gratefully acknowledged. This work was partly performed at the Swiss Light Source, Paul Scherrer Institut. Work at the University of Michigan was supported in part by U.S. Department of Energy Grant No. DE-FG02-06ER46273 and by U.S. National Science Foundation Physics Frontier Center Grant No. PHY-0114336.

*philip.willmott@psi.ch

[1] G. H. Jonker and J. H. van Santen, Physica (Amsterdam) **16**, 337 (1950).
[2] S. Jin, T. H. Tiefel, M. McCormack, R. A. Fastnacht, R. Ramesh, and L. H. Chen, Science **264**, 413 (1994).
[3] P. Schiffer, A. P. Ramirez, W. Bao, and S.-W. Cheong, Phys. Rev. Lett. **75**, 3336 (1995).
[4] A. Urushibara, Y. Moritomo, T. Arima, A. Asamitsu, G. Kido, and Y. Tokura, Phys. Rev. B **51**, 14103 (1995).
[5] C. Zener, Phys. Rev. **82**, 403 (1951).
[6] A. J. Millis, P. B. Littlewood, and B. I. Shraiman, Phys. Rev. Lett. **74**, 5144 (1995).
[7] J.-H. Liao, T.-B. Wu, S.-T. Ho, Y.-T. Chen, S.-U. Jen, and Y.-D. Yao, J. Phys. D **40**, 4586 (2007).
[8] J. Z. Sun, D. W. Abraham, R. A. Rao, and C. B. Eom, Appl. Phys. Lett. **74**, 3017 (1999).
[9] R. P. Borges, W. Guichard, J. G. Lunney, J. M. D. Coey, and F. Ott, J. Appl. Phys. **89**, 3868 (2001).
[10] P. R. Willmott *et al.*, Appl. Surf. Sci. **247**, 188 (2005).
[11] G. Koster, B. L. Kropman, G. J. H. M. Rijnders, D. H. A. Blank, and H. Rogalla, Appl. Phys. Lett. **73**, 2920 (1998).
[12] R. Herger, P. R. Willmott, O. Bunk, C. M. Schlepütz, B. D. Patterson, and B. Delley, Phys. Rev. Lett. **98**, 076102 (2007).
[13] P. R. Willmott, R. Herger, M. C. Falub, L. Patthey, M. Döbeli, C. V. Falub, M. Shi, and M. Schneider, Appl. Phys. A: Mater. Sci. Process. **79**, 1199 (2004).
[14] P. R. Willmott, R. Herger, C. M. Schlepütz, D. Martoccia, and B. D. Patterson, Phys. Rev. Lett. **96**, 176102 (2006).
[15] B. D. Patterson *et al.*, Nucl. Instrum. Methods Phys. Res. A **540**, 42 (2005).
[16] C. M. Schlepütz, R. Herger, P. R. Willmott, B. D. Patterson, O. Bunk, C. Brönnimann, B. Henrich, G. Hülsen, and E. F. Eikenberry, Acta Crystallogr., Sect. A: Found. Crystallogr. **61**, 418 (2005).
[17] R. Herger, P. R. Willmott, O. Bunk, C. M. Schlepütz, B. D. Patterson, B. Delley, V. L. Shneerson, P. F. Lyman, and D. K. Saldin, Phys. Rev. B **76**, 195435 (2007).
[18] M. Döbeli, R. M. Ender, V. Liechtenstein, and D. Vetterli, Nucl. Instrum. Methods Phys. Res. B **142**, 417 (1998).
[19] M. Döbeli, Nucl. Instrum. Methods Phys. Res. B **249**, 800 (2006).
[20] L. R. Doolittle, Nucl. Instrum. Methods Phys. Res. B **15**, 227 (1986).
[21] M. Björck and G. Andersson, J. Appl. Crystallogr. **40**, 1174 (2007).
[22] Y. Yacoby, M. Sowwan, E. Stern, J. Cross, D. Brewe, R. Pindak, J. Pitney, E. B. Dufresne, and R. Clarke, Physica B **336**, 39 (2003).
[23] D. D. Fong *et al.*, Phys. Rev. B **71**, 144112 (2005).
[24] O. Bunk, Ph.D. thesis, University of Hamburg, Department of Physics, 1999, http://www.sub.uni-hamburg.de/opus/volltexte/1999/99/
[25] The R factor used here is defined as $R(|F|)=\frac{\sum_{i=1}^{N}||F|_{i,exp}-|F|_{i,theor}|}{\sum_{i=1}^{N}|F|_{i,exp}}$, where $|F|$ is the amplitude of the structure factor.
[26] Note that PLD grows blocks of complete unit cells (i.e., ML by ML), and not layer by layer as, e.g., molecular beam epitaxy does.
[27] A. M. Haghiri-Gosnet, J. Wolfman, B. Mercey, C. Simon, P. Lecoeur, M. Korzenski, M. Hervieu, R. Desfeux, and G. Baldinozzi, J. Appl. Phys. **88**, 4257 (2000).
[28] We analyzed in addition the XRR curve of a 17-ML-thick film that confirmed the presence of an ≈20-Å-thick interface layer (although less dense). We thus can exclude that the two different optical densities shown in LSMO 6 and 9 are a result from the continuation of film growth on the STO sample 3.
[29] Note that in Fig. 2, we use the relationship $\rho=RGA/l$, where A is the film cross section, l is the distance between the electrodes, and $G=\pi/\ln(\sqrt{2})$ is a geometrical factor which accounts for the fact that the electric field lines do not run parallel through the film, but have a radial component. This factor of approximately 10 accounts for the apparent anomalously high resistivity compared to other literature values quoting the normal sheet resistivity.
[30] M. Stengel and N. A. Spaldin, Nature (London) **443**, 679 (2006).

[31] See EPAPS Document No. E-PRBMDO-77-063804 for tabulated atomic coordinates and occupation parameters in ASCII format. For more information on EPAPS, see http://www.aip.org/pubservs/epaps.html.

[32] K. Lonsdale, in *International Tables for X-Ray Crystallography*, edited by C. H. MacGillavry, G. D. Rieck, and K. Lonsdale (D. Reidel Publishing Company, Kluwer Academic Publishing, Dordrecht, 1985), Vol. III, Chap. 3.3.5, p. 232.

[33] Note that we also tried to fit the occupation parameters for the metallic sites for $z \leq -1$, but did not notice significant changes from nominal values of 0 and 1. In order to reduce the number of free parameters, we did not fit occupation parameters with $z \leq -1$.

[34] P. R. Willmott *et al.*, Phys. Rev. Lett. **99**, 155502 (2007).

[35] R. D. Shannon, Acta Crystallogr., Sect. A: Found. Crystallogr. **32**, 751 (1976).

[36] H. Dulli, P. A. Dowben, S. H. Liou, and E. W. Plummer, Phys. Rev. B **62**, R14629 (2000).

[37] R. Bertacco, J. P. Contour, A. Barthelemy, and J. Olivier, Surf. Sci. **511**, 366 (2002).

[38] J. W. Choi, J. D. Zhang, S. H. Liou, P. A. Dowben, and E. W. Plummer, Phys. Rev. B **59**, 13453 (1999).

[39] M. Izumi, Y. Konishi, T. Nishihara, S. Hayashi, M. Shinohara, M. Kawasaki, and Y. Tokura, Appl. Phys. Lett. **73**, 2497 (1998).

[40] S. Y. Liu and H. H. Kung, Surf. Sci. **110**, 504 (1981).

[41] P. R. Willmott and J. R. Huber, Rev. Mod. Phys. **72**, 315 (2000).

[42] E. Dagotto, T. Hotta, and A. Moreo, Phys. Rep. **344**, 1 (2001).

[43] W. A. Harrison, *Electronic Structure and the Properties of Solids: The Physics of the Chemical Bond* (Dover Publications, Inc., New York, 1989).

[44] H. Y. Hwang, S.-W. Cheong, P. G. Radaelli, M. Marezio, and B. Batlogg, Phys. Rev. Lett. **75**, 914 (1995).

[45] M. Medarde, J. Mesot, P. Lacorre, S. Rosenkranz, P. Fischer, and K. Gobrecht, Phys. Rev. B **52**, 9248 (1995).

[46] J. Krempaský *et al.* (unpublished).